A&A 543, A153 (2012)
DOI: 10.1051/0004-6361/201219419

Astronomy & Astrophysics

HDO and SO_2 thermal mapping on Venus: evidence for strong SO_2 variability

T. Encrenaz[1], T. K. Greathouse[2], H. Roe[3], M. Richter[4], J. Lacy[5], B. Bézard[1], T. Fouchet[1], and T. Widemann[1]

[1] LESIA, Observatoire de Paris, CNRS, UPMC, Univ. Denis Diderot, 92195 Meudon, France
e-mail: therese.encrenaz@obspm.fr
[2] SWRI, Div. 15, San Antonio, TX 78228, USA
[3] Lowell Observatory, Flagstaff, AZ 86001, USA
[4] Physics Department, University of California, Davis CA 95616, USA
[5] Department of Astronomy, University of Texas at Austin, TX 78712-1083, USA

Received 16 April 2012 / Accepted 13 June 2012

ABSTRACT

We have been using the TEXES high-resolution imaging spectrometer at the NASA Infrared Telescope Facility to map sulfur dioxide and deuterated water over the disk of Venus. Observations took place on January 10–12, 2012. The diameter of Venus was 13 arcsec, with an illumination factor of 80%. Data were recorded in the 1344–1370 cm^{-1} range (around 7.35 μm) with a spectral resolving power of 80 000 and a spatial resolution of about 1.5 arcsec. In this spectral range, the emission of Venus comes from above the cloud top (z = 60–80 km). Four HDO lines and tens of SO_2 lines have been identified in our spectra. Mixing ratios have been estimated from HDO/CO_2 and SO_2/CO_2 line depth ratios, using weak neighboring transitions of comparable depths. The HDO maps, recorded on Jan. 10 and Jan. 12, are globally uniform with no significant variation between the two dates. A slight enhancement of the HDO mixing ratio toward the limb might be interpreted as a possible increase of the D/H ratio with height above the cloud level. The mean H_2O mixing ratio is found to be 1.5 +/−0.75 ppm, assuming a D/H ratio of 0.0312 (i.e. 200 times the terrestrial value) over the cloud deck. The SO_2 maps, recorded each night from Jan. 10 to Jan. 12, show strong variations over the disk of Venus, by a factor as high as 5 to 10. In addition, the position of the maximum SO_2 mixing ratio strongly varies on a timescale of 24 h. The maximum SO_2 mixing ratio ranges between 75 +/−25 ppb and 125 +/−50 ppb between Jan. 10 and Jan. 12. The high variability of sulfur dioxide is probably a consequence of its very short photochemical lifetime.

Key words. planets and satellites: atmospheres – techniques: imaging spectroscopy – planets and satellites: composition – planets and satellites: individual: Venus

1. Introduction

The sulfur chemical cycle is known to play a key role in the atmospheric chemistry of Venus (Mills et al. 2007; Krasnopolsky 2007; Zhang et al. 2012). Below the clouds, H_2O and SO_2 are both present with mixing ratios of about 30 ppm and 100–150 ppm, respectively (Bézard & de Bergh 2007). The two species are transported above the main cloud deck by Hadley convection (Prinn & Fegley 1987). Above the cloud top, at about 65–70 km, all species are subject to photodissociation by solar UV radiation. SO_2 reacts with oxygen atoms (mostly coming from CO_2 photodissociation) to form SO_3 which reacts with H_2O to form an upper layer of H_2SO_4. The condensation of sulfuric acid feeds the main cloud at 40–65 km. The evaporation and photolysis of H_2SO_4 on the dayside is another possible SO_2 source above the clouds (Zhang et al. 2010, 2012). The abundance of H_2O above the clouds is in the range of 1–2 ppm (Fedorova et al. 2008). The SO_2 abundance above the clouds has been estimated at 10–100 ppb from Venera −15 and Pioneer Venus measurements (Zasova et al. 1993), and more recently at 100–1000 ppb by SPICAV aboard Venus Express (Marcq et al. 2011). Higher in the mesosphere, at an altitude of 80–100 km, there is evidence for an increase in the SO_2 abundance, possibly fed by a second sulfur reservoir (Sandor & Clancy 2008, 2012).

In spite of extended ground-based and space observing campaigns, the photochemistry and dynamics of the Venus mesosphere are not well undestood. UV and infrared data recorded by VeRa, VMC, SPICAV, SPICAV/SOIR and VIRTIS aboard Venus Express show evidence for latitudinal and/or temporal variations in the mesospheric temperature and pressure profiles (Tellman et al. 2009), the wind distribution at the cloud level (Hueso et al. 2012; Mc Goulrick et al. 2012), and the abundance of SO_2 above the clouds (Marcq et al. 2011; Belyaev et al. 2012). In the upper mesosphere, submillimeter observations of SO and SO_2 also show evidence for large variations in the abundances of these species (especially SO) on timescales as short as a day (Sandor et al. 2012). In addition, the long-term variation of the SO_2 abundance identified by Esposito (1984) over a timescale of several years is still not understood.

Space orbiter observations usually cover a small part of the planet with high spatial resolution at a fixed local hour. Ground-based imaging spectroscopy in the thermal infrared range provides complementary observations as it allows the simultaneous mapping of the Venus disk in a short time. It is thus best suited for studying day/night and morning/evening variations (especially near quadrature).

In this paper, we report new observations of Venus near 7 μm, obtained with the Texas Echelon-cross-Echelle Spectrograph (TEXES) at the Infrared Telescope Facility (IRTF). Data

were used to retrieve HDO and SO_2 maps of the Venus disk over a period of 48 h. Observations and modelling are described in Sect. 2. Results are presented in Sect. 3 and discussed in Sect. 4.

2. Observations and modelling

TEXES is an infrared imaging spectrometer operating between 5 and 25 μm which combines high spatial (about 1.5 arcsec) and spectral (R = 80 000) resolution (Lacy et al. 2002). Since 2001, we have been mapping the Martian disk with the TEXES instrument at IRTF, with the prime objective of detecting and mapping hydrogen peroxide, and monitoring its seasonal variations. In addition, we have been using weak transitions of HDO to monitor the water vapor simultaneously (Encrenaz et al. 2004, 2005, 2012). Our method consists of ratioing the line depths of weak neightboring transitions of minor species with respect to CO_2. It allows us to cancel, to first order, the effects associated with the calibration, the geometry, and the atmospheric parameters (Encrenaz et al. 2008). The validity of this method in the case of Venus is discussed below (Sect. 3.5).

In January 2012, we observed Venus in the 1344–1370 cm^{-1} (7.3 μm) spectral range with our main objective to map sulfur dioxide through individual transitions of its strong ν_3 band. Similar observations were performed on Mars in October 2009 and led to a stringent upper limit (0.3 ppb) for SO_2 on Mars (Encrenaz et al. 2011a). Venus was observed over three nights in 3 spectral ranges, 1350–1358 cm^{-1} (Jan. 10), 1362–1370 cm^{-1} (Jan. 11) and 1344–1352 cm^{-1} (Jan. 12). The diameter of Venus was 13 arcsec and its illumination factor was 80%. Its Doppler velocity was −10 km s^{-1}, corresponding to a Doppler shift of +0.045 cm^{-1} at 1350 cm^{-1}. The spectral resolving power was about 80 000. As in the case of our Martian observations, the 1 × 5 arcsec slit of the instrument, aligned along the North-South celestial axis, was shifted from West to East by 0.5 arcsec steps in order to map the planetary disk. Because the slit length was smaller than the Venus diameter, we had to repeat the scan 3 times in order to map the whole planet. Each scan was recorded in 10 min so a full map was obtained in 30 min. The observations were taken between 02:00 and 04:00 UT. The data were processed following the procedure used for the Mars observations (Encrenaz et al. 2004).

In this spectral range, the spectrum of Venus is dominated by a CO_2 isotopic band that probes the lower mesosphere above the cloudtop, typically at altitudes of 60–80 km. All other strong absorption features present in the TEXES spectrum are due to telluric absorption (mostly H_2O and CH_4 in the Earth's atmosphere). In what follows, we concentrate on spectral intervals outside these strong absorptions to search for trace species in the Venus mesosphere.

Figure 1 shows the spectrum of Venus integrated over the whole disk in two specific intervals: 1350.0–1350.8 cm^{-1} (Jan. 10) and 1366.3–1367.0 cm^{-1} (Jan. 11). The synthetic spectrum of Venus, shifted by +0.045 cm^{-1}, is shown for comparison, with absorptions due to CO_2, HDO and SO_2. Synthetic spectra of Venus were calculated using a radiative transfer line-by-line code adapted from our Mars analysis (Encrenaz et al. 2004) to fit the VIRTIS-H/Venus Express data of tropospheric CO in the (1–0) band at 4.7 μm (Encrenaz et al. 2011b). Spectroscopic data were taken from the GEISA data bank (Jacquinet-Husson et al. 2009). The thermal profile was derived from our anaysis of the VIRTIS data in the CO band at 4.7 μm which also probes the atmosphere above the cloud top. This model assumes a cloud top of infinite opacity at 60 km, with a cloud top temperature of 235 K and a pressure of 100 mbar at this level. The temperatures

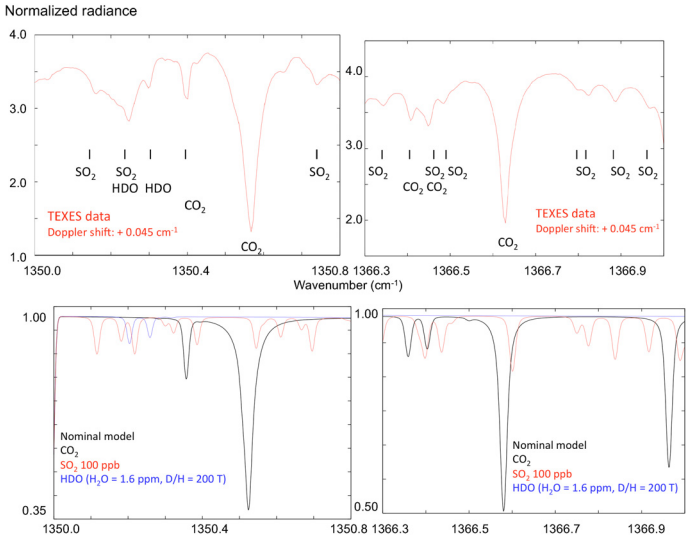

Fig. 1. *Top*: two spectra of Venus recorded by TEXES, integrated over the whole disk, covering the 1350–1350.8 cm^{-1} range (*left*) and the 1366.3–1370.0 cm^{-1} range (*right*). The weak, broad absorption band at 1350.20–1350.3 cm^{-1} is due to telluric absorption. *Bottom*: a model of the Venus mesosphere including transitions of CO_2 (black line), HDO (blue line) and SO_2 (red line), shifted by +0.045 cm^{-1}, in the same spectral ranges. Two HDO lines and several SO_2 lines are easily identified in the Venus spectra.

are 218 K and 192 K at altitudes of 70 km and 80 km, respectively (Encrenaz et al. 2011b). In the 60–80 km region probed by the weak lines of the TEXES spectrum, little systematic difference is expected between the day side and the night side (Seiff et al. 1980), so the same profile can be used over the whole Venus disk. It can be seen from Fig. 1 that the nominal profile used in our calculations gives a reasonable overall fit of the CO_2 absorptions, with CO_2 line depths of about 20% at 1340.4 cm^{-1} and 65% at 1350.58 cm^{-1} (Doppler-shifted frequencies). We note, anyway, that the temperature profile used in Fig. 1 is not optimized to fit the CO_2 lines of the TEXES spectra. We use it as a first-order guess to model the HDO and SO_2 lines whose depths are about the same as the weak CO_2 lines. As shown in Fig. 1, two lines of HDO are identified at 1350.25 and 1350.30 cm^{-1} (Doppler-shifted frequencies). Several transitions of SO_2 are unambiguously identified in both spectral ranges with several dozen SO_2 transitions also identified over the whole spectral range. Two other HDO transitions are also found in the 1344–1345 cm^{-1} range.

Figure 2 shows the weighting functions in three transitions used in the present study for retrieving HDO and SO_2 maps: HDO at 1350.30 cm^{-1}, SO_2 at 1350.16 cm^{-1} and CO_2 at 1350.40 cm^{-1} (Doppler-shifted frequencies). It can be seen that all three weighting functions peak in the 65–75 km altitude range.

3. Results

3.1. Continuum and CO_2

Figure 3a shows the maps of the continuum at 1350.3 cm^{-1} (on each side of the 1350.3 cm^{-1} CO_2 line) retrieved for Jan. 10 and Jan. 12. It can be seen that the maps are globally isotropic with some limb-darkening effect, with no evidence for local structures. In the continuum map of Jan. 10, there is a slight flux increase on the dayside limb. There is no evidence for a

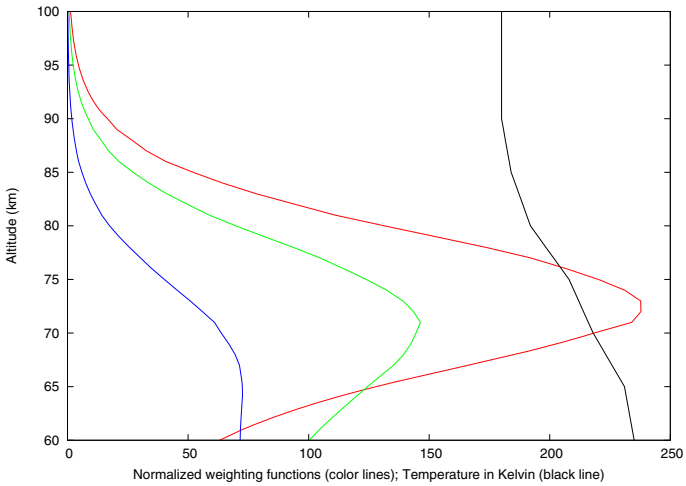

Fig. 2. Weighting functions in the Venus atmosphere for three weak transitions used in our calculations: (red) CO_2 at 1350.40 cm^{-1}, (green) SO_2 at 1350.16 cm^{-1}, and (blue) HDO at 1350.30 cm^{-1} (Doppler-shifted frequencies). The mixing ratios of SO_2 and H_2O are, respectively, 100 ppb and 1 ppm (with D/H = 200 times the terrestrial ratio). Black line: temperature vertical profile.

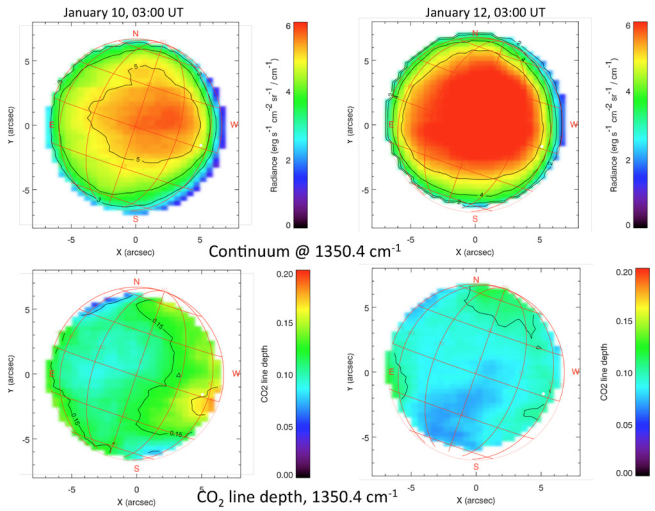

Fig. 3. a) *Top*: map of the continuum of Venus at 1350.3 cm^{-1}, on Jan. 10 (*left*) and Jan. 12 (*right*). The subsolar point is indicated by a white dot. The night side corresponds to the left limb of the planet. **b)** *Bottom*: map of the continuum of the CO_2 line at 1350.40 cm^{-1} (Doppler-shifted frequency) on Jan. 10 (*left*) and Jan. 12 (*right*).

latitudinal effect, even at high latitude. A surprising result is the change in absolute scale between the two maps, with an increase of about 15% on Jan. 12. A possible explanation is a change in telluric transmission or some uncertainty in the absolute calibration, discussed in Sect. 4.1.

Figure 3b shows the maps of the CO_2 line depth at 1350.3 cm^{-1} for Jan. 10 and Jan. 12. The general shape of the map is similar, with a maximum on the right limb (near the subsolar point) and a second local maximum on the left limb (night side). We verified that we reproduce this general shape well using other weak CO_2 features. The increase toward the limb is partly due to the airmass effect. Surprisingly, the depth of the CO_2 line is noticeably weaker, by about 30%, on Jan. 12; assuming a constant temperature gradient, we would have expected the temperature increase shown in Fig. 3a would signal a corresponding increase in the cloud pressure. Again, this

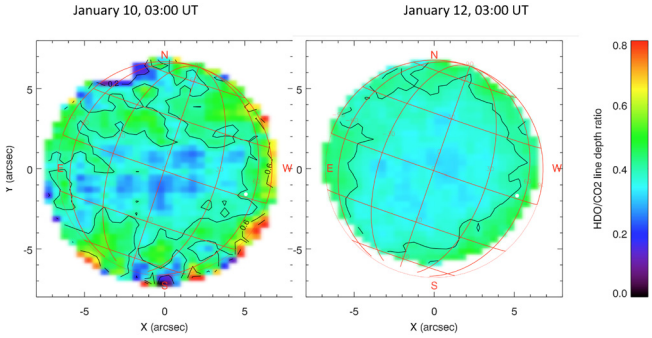

Fig. 4. Map of the HDO/CO_2 line depth ratio derived from the 1350.30 cm^{-1} HDO line and the 1350.40 cm^{-1} CO_2 line (Doppler-shifted frequencies). *Left*: January 10, 2012; *right*: January 12, 2012. The subsolar point is indicated with the white spot. A depth ratio of 0.4 corresponds to a H_2O mixing ratio of 1.5 ppm, assuming a D/H ratio of 200 (see text, Sect. 3.4).

effect depends on the TEXES absolute calibration, whose accuracy might have to be verified (see Sect. 4.1).

3.2. HDO

The HDO maps were obtained using two HDO transitions, at Doppler-shifted frequencies of 1344.95 cm^{-1} (Jan. 12) and 1350.30 cm^{-1} (Jan. 10 and 12, respectively), and the corresponding CO_2 transitions, at 1345.25 cm^{-1} (Jan. 12) and 1350.40 cm^{-1} (Jan. 10 and 12, respectively). On Jan. 12, both line sets led to identical maps. Figure 4 shows the HDO maps obtained at 1350 cm^{-1} on Jan. 10 and 12. Both maps show a rather uniform spatial distribution, with variations less than about +/−20%. Temporal variations are globally less than 10% over 48 hours. The HDO map shows some limb brightening, discussed in more detail in Sect. 4.

3.3. SO_2

The SO_2 maps were obtained using two sets of transitions at the following Doppler-shifted frequencies: (1) SO_2 at 1350.16 cm^{-1} and CO_2 at 1350.40 cm^{-1} (Jan. 10 and 12); (2) SO_2 at 1366.48 cm^{-1} and CO_2 at 1366.41 cm^{-1} (Jan. 11). The SO_2 and CO_2 lines used on Jan. 11 are, respectively, stronger and weaker than the ones used on Jan. 10. As a result, the SO_2/CO_2 line depth ratio is about 3 times larger on Jan. 11 for the same SO_2 mixing ratio. Using other SO_2 transitions in a given night gave the same maps. Figure 5 shows the SO_2 maps obtained at 1350 cm^{-1} (Jan. 10 and 12) and 1366 cm^{-1} (Jan. 11). In contrast with the HDO lines, the SO_2 maps vary by factors as much as 5 on Jan. 12 and 10 on Jan. 10 and 11. The shape of the SO_2 map is also strongly variable from one night to another. As will be shown below, the maximum SO_2 abundance shows a moderate change between Jan. 10 and 12. There is no evidence for a day-night effect, nor for a systematic latitudinal effect. The three maps are discussed in more detail in Sect. 4.

3.4. Retrieval of HDO and SO_2 mixing ratios

We have modelled the spectrum of Venus in two spectral ranges, the 1350.10–1350.45 cm^{-1} range (Jan. 10), and the 1366.30–1366.50 cm^{-1} range (Jan. 11). In each case, we have isolated two areas in the disk of Venus, Area 1 where the SO_2 line is strongest (also corresponding to a maximum

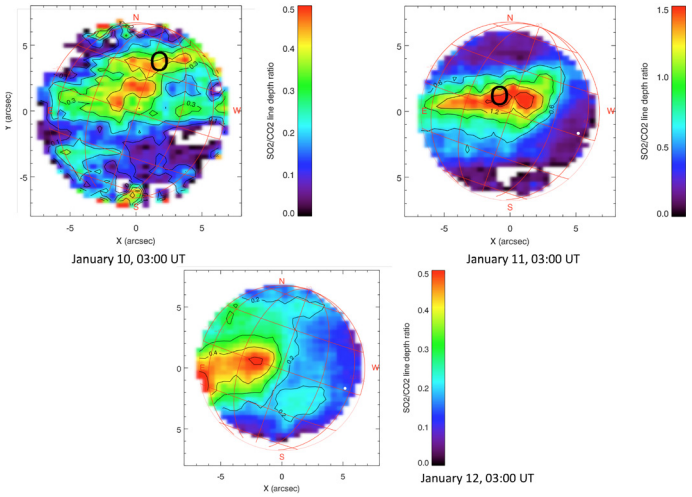

Fig. 5. Map of the SO_2/CO_2 line depth ratio derived from the 1350.16 cm^{-1} SO_2 line and the 1350.40 cm^{-1} CO_2 line (Jan. 10 and 12) and the 1366.48 cm^{-1} SO_2 line and the 1366.41 cm^{-1} CO_2 line (Jan. 11). All frequencies correspond to Doppler-shifted transitions. On Jan. 10 and 11, Area 1 (maximum SO_2 line depth) is indicated by a black circle. Area 2 (maximum CO_2 line depth) is located around the subsolar point, which is indicated by the white spot. At 1350 cm^{-1} (Jan. 10 and 12), a depth ratio of 0.45 corresponds to a SO_2 mixing ratio of 60 ppm. At 1366 cm^{-1} (Jan. 11), a depth ratio of 1.5 corresponds to a SO_2 mixing ratio of 100 ppm. (see text, Sect. 3.4).

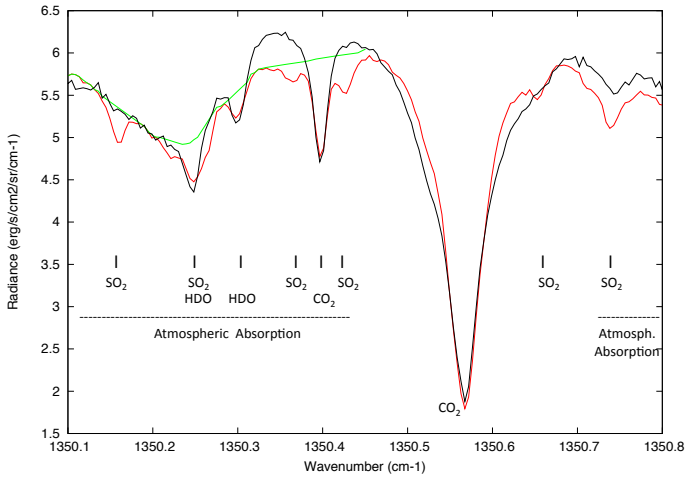

Fig. 6. The TEXES spectra on Jan. 10 in (red) Area 1 (maximum SO_2) and (black) Area 2 (maximum CO_2), in the 1350.10–1350.80 cm^{-1} spectral range. The telluric absorption is indicated by a green line. The absolute scale of the spectrum in Area 2 has been normalized to the one of Area 1 for comparison. It can be seen that SO_2 is not detected in Area 2. At 1350.41 cm^{-1}, the CO_2 transition is deeper, mostly due to the higher air mass.

SO_2/CO_2 mixing ratio) and Area 2 (around the subsolar point) where the CO_2 line depth is strongest (also associated with a minimum SO_2/CO_2 mixing ratio). Figure 6 shows the spectra in both areas on Jan. 10 between 1350.0 and 1350.8 cm^{-1}, integrated over 12 pixels in each area. Terrestrial absorption in the TEXES spectrum is also shown in Fig. 6. It can be seen that all the SO_2 lines are clearly visible in Area 1, while they are not detectable in Area 2. Figure 7 shows the fit of the spectrum in Area 1 corrected for terrestrial absorption with a set of synthetic models. We first adjusted the thermal profile and the convolution (0.016 cm^{-1}) to fit the CO_2 line at 1350.4 cm^{-1} (Doppler-shifted

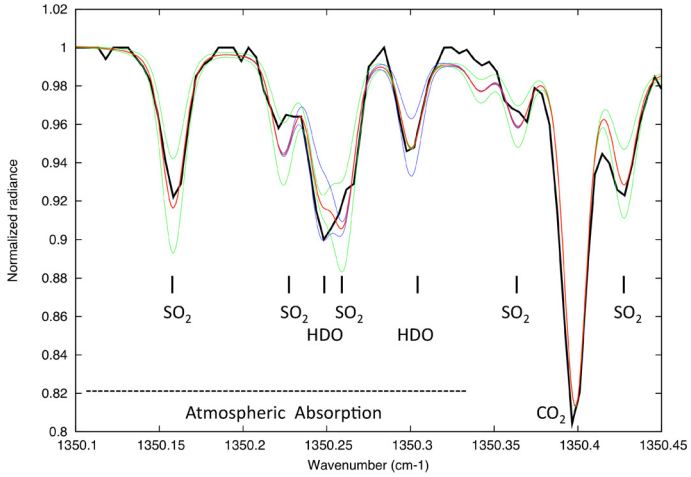

Fig. 7. Black thick line: the TEXES spectrum of Jan. 10 in Area 1 (maximum SO_2) corrected for atmospheric absorption, in the 1350.10–1350.45 cm^{-1} spectral range. Thin lines: synthetic models. Red curve: best fit (H_2O = 1.5 ppm, SO_2 = 75 ppb). Blue curves: SO_2 = 75 ppb, H_2O = 1.0 (upper curve) and 2.0 ppm (lower curve). Green curves: H_2O = 1.5 ppm, SO_2 = 50 ppb (upper curve) and 100 ppb (lower curve).

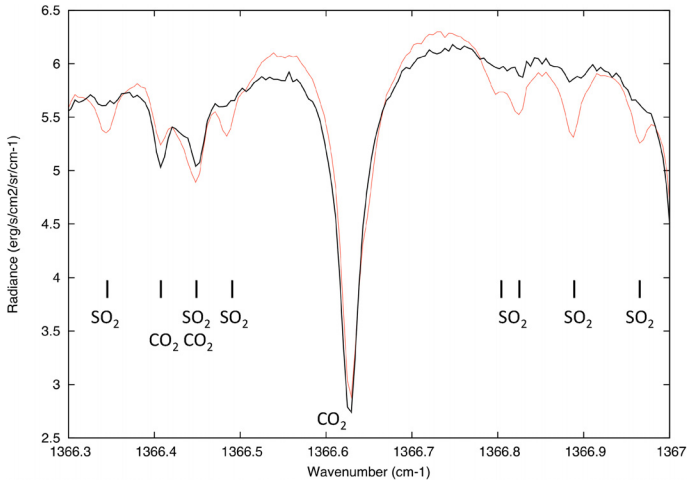

Fig. 8. a) Solid line: the TEXES spectrum on Jan. 11 in (red) Area 1 (maximum SO_2) and (black) Area 2 (maximum CO_2), in the 1366.30–1370.0 cm^{-1} spectral range. The SO_2 lines are very marginally detected in Area 2. At 1366.4 cm^{-1}, the stronger depth of the CO_2 transition is mostly due to the higher air mass of Area 2.

frequency). The best fit is obtained for a H_2O mixing ratio of 1.5 +/−0.75 ppm, assuming a D/H mixing ratio of 200 times the terrestrial value, and a SO_2 mixing ratio of 75 +/−25 ppb. Figure 8 shows the spectra of Areas 1 and 2 for Jan. 11 in the 1366.30–1367.0 cm^{-1} region, and Fig. 9 shows the fit of the 1366.3–1366.5 cm^{-1} spectral range with synthetic models, after using a 1st-order polynomial to correct the slope of the TEXES spectrum. In order to fit the CO_2 transition at 1366.40 cm^{-1}, we had to adjust the convolution to 0.018 cm^{-1} and to increase the pressure at the cloud top to 150 mbar. (We note that the CO_2 line could also have been fitted using the pressure of 100 mbar at the cloudtop (as for Jan. 10) and a slightly larger temperature gardient above the clouds; we have no way to discriminate between these two profiles, but both lead to the same synthetic lines for HDO and SO_2.) The best fit is obtained for a SO_2 mixing ratio of 125 +/−50 ppb. The estimate of the error bars is discussed below (Sect. 3.6).

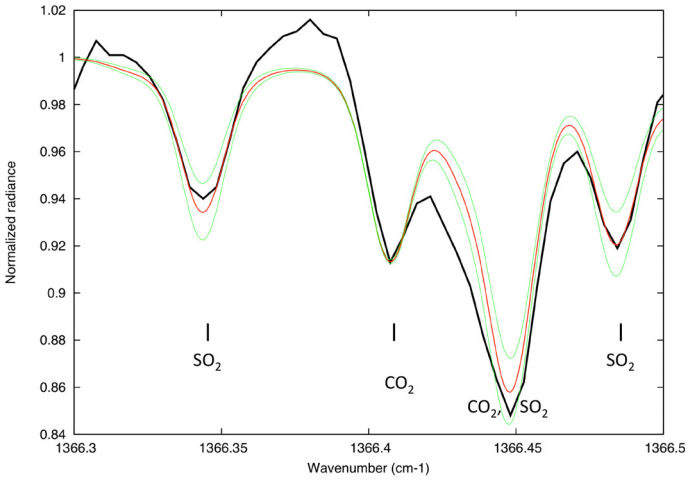

Fig. 9. Black thick line: the TEXES spectrum of Jan. 11 in Area 1 (maximum SO_2) in the 1366.30–1366.50 cm^{-1} spectral range, after removal of the continuum slope by a 1st-order polynomial. Thin lines: synthetic models corresponding to different SO_2 mixing ratios. Red curve: best fit (SO_2 = 125 ppb). Green curves: SO_2 = 100 ppb (upper curve) and 150 ppb (lower curve).

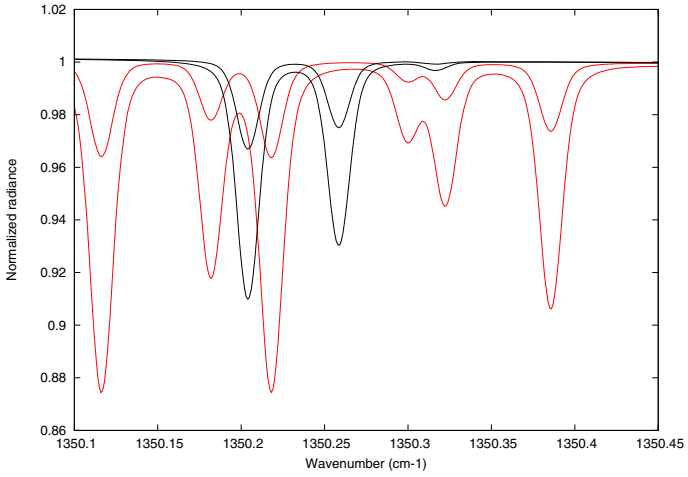

Fig. 10. The synthetic spectrum of SO_2 and HDO on Venus between 1350.10 and 1350.45 cm^{-1} (rest frequencies). Red: SO_2 = 25 ppb (upper curve) and 100 ppb (lower curve). Black: HDO = 1 ppm (upper curve) and 3 ppm (lower curve). For the SO_2 line at 1350.12 cm^{-1}, the line depths are 0.035 and 0.126 respectively; the departure from linearity is 11%. For the HDO line at 1350.26 cm^{-1}, the line depths are 0.025 and 0.070 respectively; the departure from linearity is 7%. Spectra are calculated with a mean airmass of 1.4.

3.5. Validity of the mapping method

For retrieving the SO_2/CO_2 and HDO/CO_2 maps, we have assumed that the line depths of the SO_2, HDO and CO_2 lines used in our calculations vary linearly with the mixing ratios of the species. In the case of Mars, we have shown that the method is valid for line depths weaker than about ten percent (Encrenaz et al. 2008). Figure 10 illustrates the validity of our method in the case of Venus. The 1350.10–1350.45 cm^{-1} synthetic spectrum of HDO and SO_2 on Venus is shown for mixing ratios of 1 and 3 ppm for H_2O, and 25 and 100 ppb for SO_2. We find that, for the two transitions used for Figs. 4 and 5, linearity holds to 7% for HDO (1350.30 cm^{-1}) and 12% for SO_2 (1350.16 cm^{-1}). As discussed below (Sect. 3.6), this is significantly smaller than the uncertainty associated with the continuum definition.

3.6. Uncertainties on the mixing ratios

We identify several possible sources of error in the retrieval of the HDO and SO_2 mixing ratios. Two of them are instrumental: the limitation due to the noise level of the data, and the uncertainty due to the definition of the continuum level. A third source of uncertainty is linked with the absolute calibration and the fourth one is associated with the atmospheric model used for the synthetic spectra. Error from the absolute calibration should be negligible because our mixing ratios are inferred from line depths ratios, which are not affected by the absolute calibration. Error from atmospheric model has been estimated to less than 15% (Sect. 3.5). The signal to noise of the TEXES spectra has been estimated using the identification of very weak SO_2 lines and the measurement of the continuum fluctuations. The disk-integrated spectra shown in Fig. 1, integrated over about 800 pixels each, have a continuum level of about 4 erg s^{-1} cm^{-2} sr^{-1}/cm^{-1} and has a 2-σ signal to noise ratio of about 700 per convolution element in the continuum. The spectrum of Area 1 shown in Fig. 6, integrated over 12 pixels, corresponds to a continuum level of 5 erg s^{-1} cm^{-2} sr^{-1}/cm^{-1} and has a 2-σ signal to noise ratio of about 100. The same S/N applies for the Jan. 11 data (Fig. 8). It appears clearly from Figs. 6 and 8 that the uncertainty on the continuum level is the main source of error. This uncertainty has two origins: the terrestrial atmospheric absorption (Figs. 6) and the instrumental error associated with the continuum (Figs. 8 and 9). The atmospheric absorption is continuously recorded by the TEXES instrument in parallel with the Venus data, but there is still some uncertainty associated with it, especially for strong absorption bands. These two sources of uncertainty are responsible for the poor fits observed, in particular, around 1350.33 cm^{-1} in Fig. 7 and around 1366.38 cm^{-1} in Fig. 9. We determine the error bars taking into account these discrepancies. In the case of HDO, the fit of the whole 1350.10–1350.45 cm^{-1} range leads to a H_2 mixing ratio of 1.5 ppm (with D/H = 200 times the terrestrial value). However, if we consider only the HDO line at 1350.3 cm^{-1}, taking into account the continuum discrepancy, the best fit would correspond to a H_2O mixing ratio of 2.0 ppm. We thus derive a H_2O/CO_2 mixing ratio of 1.5 +/−0.75 ppm. In the case of SO_2, both the single line fit at 1350.15 cm^{-1} and the whole 1350.10–1345.0 cm^{-1} region fits lead to the same SO_2 mixing ratio. We thus derive a SO_2 mixing ratio of 75 +/−25 ppb. For the Jan. 11 data set (Fig. 9), fitting the whole 1366.30–1366.50 cm^{-1} region leads to a value of 125 ppb, while the SO_2 line at 1366.35 cm^{-1} would be best fitted with a SO_2 mixing ratio of 150 ppb. We conclude that the SO_2 maximum mixing ratio for the Jan. 12 data set is 125 +/−50 ppb.

4. Discussion

4.1. Continuum and CO_2 line depth maps

Figure 3a shows that the TEXES continuum maps are globally symmetric with respect to the disk center, with a limb darkening effect as expected for a temperature structure which decreases as the altitude increases above the cloud. There is a possible warming on the day side on Jan. 10, consistent with the proximity of the subsolar point. There is no noticeable latitudinal variation in the continuum maps. Even near the poles, individual spectra do not show any signature of inversion above the cloud-top, as identified in particular by the VIRTIS data at 4.5–5 μm (Grassi et al. 2008; Encrenaz et al. 2011b). The reason is probably the limited spatial resolution of TEXES (1.5 arcsec) which

does not allow us to resolve latitudes higher than 75°. A surprising result is the change of intensity in the entire central region within a 48 h timescale. As mentioned above, the flux increases by 15% between Jan. 10 and Jan. 12. The flux measured on Jan. 11, if rescaled at 1350.3 cm^{-1}, indicates an intermediate value. Assuming the absolute calibration of TEXES is correct, and no change in the atmospheric transmission, the measured radiances would correspond to brightness temperatures ranging from 226 K on Jan. 10 to 230 K on Jan. 12. The temperature range is in good agreement with the measurements recorded by the infrared camera of Akatsuki which indicate a temperature range of 225–240 K in the 8–12 μm range (Fukuhara 2012). However, a change by 4 K in 48 hours appears unlikely. Millimeter measurements of the telluric water content on Jan. 10 and 12 at the time of our observations indicate that the atmospheric transmission was better and more stable on Jan. 12 than on Jan. 10; this change might be at least partly responsible for the observed effect.

The depth of the CO_2 line at 1350.3 cm^{-1} is weaker by about 30% on Jan. 12 than on Jan. 10 (Fig. 3b). In contrast, fitting the 1366.4 cm^{-1} CO_2 line on Jan. 11 indicates that, if the temperature profile is unchanged, the pressure of the cloud top is 150 mbar, higher than on Jan. 10 by 50%. These differences in temperature and pressure are surprising, as we would have expected, assuming no change in the temperature gradient, that the temperature and the pressure at the cloud top would be correlated. We have to note, however, that the fit of the 1366.4 cm^{-1} CO_2 line can also be obtained by a slight increase of the temperature gradient above the cloudtop. A more complete analysis of the TEXES data regarding the cloud structure and temperature profile will be presented in a forthcoming publication. For the present study, we simply choose temperature and pressure vertical distributions which fit the CO_2 weak transitions (knowing that these distributions are not unique solutions), and we apply them to model the HDO and SO_2 lines.

4.2. HDO

The two HDO maps recorded on Jan. 10 and Jan. 12 show little variability over the disk, with differences less than a factor of two. There is no evidence for a day-night or a noon-evening variation. The only noticeable effect is limb brightening, especially visible on Jan. 12 and also visible on the 1344.9 cm^{-1} (Doppler-shifted frequency) HDO map. This effect seems to indicate that the HDO/CO_2 ratio is increasing with altitude above the clouds. A possible explanation could be that the H_2O mixing ratio is constant and the D/H ratio is increasing with altitude. The D/H ratio below the clouds has been measured as 0.0187 +/−0.0062, i.e. 120 +/−40 times the terrestrial value in the troposphere using near-infrared spectroscopy in the night side (Bézard et al. 1990; de Bergh et al. 1991), and 157 +/−30 using Pioneer Venus data (Donahue et al. 1997). However, the values inferred in the mesosphere by SPICAV aboard Venus Express are significantly higher, in the range of 200 times the terrestrial value or even more (Fedorova et al. 2008). These measurements, inferred from solar occultation data, show a large variation over time, location and altitude. SPICAV data seem to indicate a slight increase of HDO/H_2O with altitude between 75 and 95 km (Bertaux et al. 2007). Liang et al. (2009) interpret this effect as possibly due to photo-induced isotopic fractionation or to hydrogen escape. Monitoring the HDO spatial distribution over the Venus disk will be an interesting complementary method to address this issue. Determining the D/H vertical distribution from the TEXES data will require an accurate determination of the thermal profile. We plan to address this issue in a forthcoming publication.

The mean H_2O mixing ratios inferred by the TEXES data on Jan. 10 and 12, assuming a D/H ratio of 200 times the terrestrial value, are consistent with previous measurements above the clouds from space (Fedorova et al. 2008; Cottini et al. 2012) and from the ground (Krasnopolsky 2010; Matsui et al. 2012). Fedorova et al. (2008), using solar occultation infrared spectroscopy with SPICAV/SOIR aboard Venus Express, derived mean mixing ratios of 1.16 +/−0.24 ppm and 0.086 +/−0.020 ppm respectively at an altitude level of 70–95 km; the inferred mean D/H ratio is 240 +/−20 times the terrestrial value. Using VIRTIS-H/VEx data around 2.55 μm, Cottini et al. (2012) derived a H_2O mixing ratio of 3 +/−1 ppm above the clouds. Using ground-based high-resolution spectroscopy of HDO lines at 3.7 μm, Krasnopolsky (2010) derived a H_2O mixing ratio ranging from 1.2 ppm at mid-latitudes to 2.9 ppm at +/−75° latitudes, assuming a D/H ratio of 200 times the terretsrial value. Matsui et al. (2012), using ground-based near-infrared spectroscopy ar 2.3 μm on the day side of Venus, find a disk-integrated HDO mixing ratio of 0.22 +/−003 ppm, which translates into a H_2O mixing ratio of 3.4 ppm if a D/H ratio of 200 times the terrestrial value is used. All these results agree reasonably well with the TEXES results, taking into account the local and temporal variations reported by the authors.

4.3. SO_2

The SO_2 maps in Fig. 4 show very strong variations, both spatially in each map and temporally over a time scale of 2 days. The maps of Jan. 10 and 11 show local variations of as much as a factor of 10, and the Jan. 12 map shows variations by a factor of about 5. Another surprising result is the change in the position of the SO_2 maximum. On Jan. 10, the region of maximum SO_2 abundance shows a multi-structured pattern, located in the northern hemisphere on the day side. On Jan. 11, this maximum changes into a double structure located in the vicinity of the equator, still on the day side. On Jan. 12, the two maximum spots are located toward the night side at mid-southern latitudes. If we assume that the same SO_2 feature is moving at the cloud level, then very strong winds are required. Indeed the maximum SO_2 spots of Jan. 10 and Jan. 12 are separated by about 45° West longitude and 45° South latitude, which would imply winds of about 25–30 m/s both in the zonal and meridional directions. Such estimates are inconsistent with wind measurements obtained at the cloud level which indicate, in particular, very weak meridional winds at mid-latitudes (lower than 10 m/s; Hueso et al. 2012). A more likely explanation is related to the very short photochemical timescale of SO_2. Hot spots of sulfur dioxide could come to the cloudtop level from small convective cells and would disappear over a short period of time due to photodissociation and/or formation of SO_3. Small convective cells near the equator could explain the vertical transport of SO_2, as convective vertical mixing dominates at low latitudes (e.g. Titov et al. 2008). Below the clouds, the SO_2 mixing ratio is higher than 100 ppm. As pointed out by Marcq et al. (2011) and Marcq (2012), the injection of a small excess (by about 1%) at the equator would be sufficient to generate a mesospheric SO_2 latitudinal distribution with mixing ratios in the range of a few tens ppb, which would be consistent with the values inferred by TEXES.

The maximum values of the SO_2 mixing ratio derived from the TEXES data can be compared with other recent measurements of the same altitude. Using UV data from SPICAV/VEx in the nadir mode, Marcq et al. (2011) derived, at mid-latitudes,

SO_2 abundances ranging between 5 and 50 μm-atm, which translate into mixing ratios of 100 ppb–1 ppm at an altitude of 70 km. Belyaev et al. (2012), using SPICAV/SOIR in the solar occultation mode, inferred, at an altitude of 65 km, SO_2 mixing ratios decreasing from 0.2–0.5 ppm at the equator down to 0.05–0.1 ppm in the North polar region. Using ground-based near-infrared spectroscopy, Krasnopolsky (2010) reported a mean SO_2 mixing ratio of 350 +/−50 ppb. The TEXES results are lower than those reported by Krasnopolsky (2010) and Marcq et al. (2011), but are consistent with those of Belyaev et al. (2012). They are also in reasonable agreement with older results inferred from Venera-15 and Pioneer Venus measurements that range from a few tens ppb at low and mid-latitudes to a few hundreds of ppb at high latitudes (Zasova et al. 1993). All studies illustrate the high variability of SO_2 on both short and long time scales.

In conclusion, the present analysis illustrates the capability of ground-based imaging spectroscopy for complementing space data and better constraining the short-term variability of sulfur dioxide. Repeating this observing program near quadrature will allow us to better constrain possible day-night effects. Simultaneous observations of the SO_2 ν_3 band at 7 μm, the SO_2 ν_2 band at 19 μm, and possibly also the SO_2 ν_1 band at 8.7 μm, should allow us to retrieve information about the scale height of sulfur dioxide at the cloud level. Indeed, this method was successfully used by Zasova et al. (1993) on Venera-15 data that had a spectral resolution of 5–7 cm^{-1}. The high spectral resolving power of TEXES should allow us to obtain instantaneous maps of the SO_2 scale height, and, possibly, better understand the relationship between the SO_2 local variations and the cloud structure.

Acknowledgements. T.E., T.K.G. and H.R. were visiting astronomers at the Infrared Telescope Facility, which is operated by the University of Hawaii under Cooperative Agreement no. NNX-08AE38A with the National Aeronautics and Space Administration, Science Mission Doctorate, Planetary Astronomy Program. We thank the IRTF staff for the support of TEXES observations. Observations with TEXES were supported by NSF Grants AST-0607312 for JHL and AST-0708074 for MJR. T.K.G. acknowledges support by NASA Grant NNX08AW33G S03 for data reduction. T.E. and B.B. acknowledge support from CNRS, and T.F. aknowledges support from UPMC and IUF. T.E. and T.W. acknowledge support from the Programme National de PlanÃl'tologie. We thank E. Marcq for helpful discussions regarding this paper.

References

Belyaev, D. A., Korablev, O., Fedorova, A., et al. 2008, J. Geophys. Res., 113, E00B25
Belyaev, D. A., Montmessin, F., Bertaux, J.-L., et al. 2012, Icarus, 217, 740
Bertaux, J.-L., Vandaele, A.-C., Korablev, O., et al. 2007, Nature, 450, 646
Bézard, B., & de Bergh, C. 2007, J. Geophys. Res., 112, E04S07
Bézard, B., de Bergh, C., Crisp, D., & Maillard, J.-P. 1990, Nature, 345, 508
Cottini, V. Igniatiev, N., Piccioni, G., et al., 2012, Icarus, 217, 561
de Bergh, C., et al. 1991, Science, 251, 547
Donahue, T. M., Grinspoon, D. H., Hartle, R. E., & Hodges, R. R. 1997, in Venus II: Geology, Geophysics, Atmosphere and Solar Wind, eds. S. W. Bougher et al. (University of Arizona Press), 385
Encrenaz, T., Bézard, B., Greathouse, T. K., et al. 2004, Icarus, 170, 424
Encrenaz, T., Bézard, B., Owen, T., et al. 2005, Icarus, 179, 43
Encrenaz, T., Greathouse, T. K., Richter, M. J., et al. 2008, Icarus, 195, 547
Encrenaz, T., Greathouse, T. K., Richter, M. J., et al. 2011a, A&A, 530, A37
Encrenaz, T., Drossart, P., Erard, S., et al. 2011b, Communication presented at the EPSC-DPS Conference, Nantes, October 3–7
Encrenaz, T., Greathouse, T. K., Lefevre, F., & Atreya, S. K. 2012, Plan. Space Sci., in press
Esposito, L. W. 1984, Science, 223, 1072
Fedorova, A. A., Rodin, A. V., & Baklanova, I. V. 2004, Icarus, 171, 54
Fedorova, A., Korablev, O., Vandaele, A.-C., et al. 2008, J. Geophys. Res., E00B25
Fukuhara, T. 2012, Communication presented at the Sakura/Europlanet Workshop Venus as a Transiting Planet, Paris, March 5–7
Grassi, D., Drossart, P., Piccioni, G., et al. 2008, J. Geophys. Res., E00B25
Hueso, R., Peralta, J., & Sanchez-Lavega, A. 2012, Icarus, 217, 585
Jacquinet-Husson, N., Scott, N., Chedin, A., et al. 2008, J. Quant. Spectr. Rad. Transfer, 109, 1043
Krasnopolsky, V. A. 2007, Icarus, 191, 25
Krasnopolsky, V. A. 2010, Icarus, 209, 314
Lacy, J. H., Richter, M. J., Greathouse, T. K., et al. 2002, PASP, 114, 153
Liang, M. C., & Yung, Y. L. 2009, J. Geophys. Res., 114, E00B28
Marcq, E. 2012, Communication presented at the Sakura/Europlanet Workshop Venus as a Transiting Planet, Paris, March 5–7
Marcq, E., Belyaev, D. A., Montmessin, F., et al. 2011, Icarus, 211, 58
Matsui, H., Iwagami, N., Hosouchi, M., et al. 2012, Icarus, 217, 610
Mills, F. P., Esposito, L. W., & Yung, Y. K. 2007, Atmospheric composition, chemistry and clouds, in Exploring Venus as a Terrestrial Planet, Geophysical Monograph Serires, 176, 73
Sandor, B. J., Clancy, R. T., Moryarty-Schieven, G. H., & Mills, F. P. 2010, Icarus, 208, 49
Seiff, A., Kirk, D. B., Young, R. E., et al. 1980, J. Geophys. Res., 85, 7903
Tellmann, S., Patzold, M., Hausler, et al. 2009, J. Geophys. Res., E00B36
Titov, D.V., Taylor, F. W., Svedem, H., et al. 2008, Nature, 456, 620
Zhang, X., Liang, M.-C., Montmessin, F., et al. 2010, Nature Geosc. Lett., 3, 834
Zhang, X., Liang, M. C., Mills, F. P., et al. 2012, Icarus, 217, 714
Zasova, L. V., Moroz, V. I., Esposito, L. W., & Na, C. Y. 1993, Icarus, 105, 92